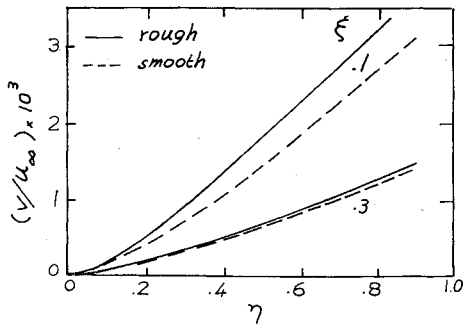

Fig. 4 Distribution of radial velocity component.

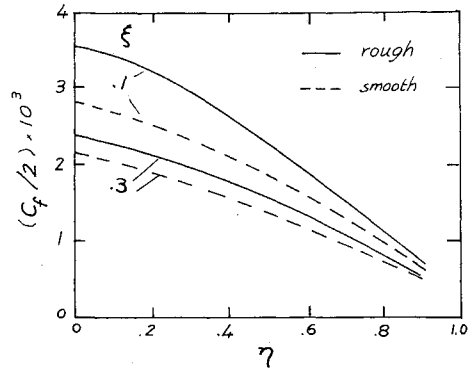

Fig. 5 Distribution of shear.

located. By means of appropriate mass and momentum balances, the skin friction and the distributions of the radial velocity component and the shear stress throughout the boundary layer were calculated.[3] The foregoing procedure was repeated on an identical cylinder but having a smooth surface. Freestream conditons were about the same in both cases, including a velocity of 104 fps and a Reynolds number per inch of 4.7×10^4. By comparing the results of measurements on the rough and smooth cylinders, the effects of surface roughness could be distinguished.

From Fig. 1, surface roughness increases all boundary-layer thicknesses by up to 15%. The percentage increase is more pronounced near the forward part of the model than toward the end. This agrees with the fact that roughness effects should decrease along the model, since the magnitude of the surface depressions relative to the boundary-layer thickness decreases due to boundary-layer growth along the model.

Figures 2a and 2b show the axial velocity profiles for the smooth and rough cylinders, respectively. Both agree closely with the Klebanoff and Diehl profile[4] for a smooth flat plate, except that near the rough wall the velocity is somewhat smaller than the smooth wall for a given value of (y/δ^*).

The average skin friction for the rough and smooth cylinders is compared in Fig. 3. It is seen that surface roughness increases the skin friction by up to about 15% and that its effect tends to diminish along the cylinder. Also, the skin friction for the smooth cylinder appears to be in satisfactory agreement with the Prandtl-Schlichting relation for a smooth flat plate, indicating that transverse curvature effects are neglible. This conclusion agrees with the predictions of transverse curvature effects in Ref. 5. The foregoing remarks also apply to the local skin friction.

Because of the cylindrical geometry, the distributions of the radial velocity and shear throughout the boundary layer depend on the boundary-layer thickness relative to the cylinder radius. Both distributions are shown in Figs. 4 and 5, respectively. Surface roughness increases the radial velocity component for a given boundary-layer thickness and distance from the wall. The percentage increase becomes smaller as the boundary layer grows, i.e., as the ratio of the depressions relative to boundary-layer thickness diminishes. Similar observations apply to the shear.

It may be concluded that relatively small values of surface roughness of the order reported here cause substantial increases in the thickness of the turbulent boundary layer and skin friction. Furthermore, surface roughness effects extend throughout the entire boundary layer and, in particular, modify the distributions of the radial velocity component and the shear.

References

[1] Clauser, F. H., *Advances in Applied Mechanics* (Academic Press Inc., New York, 1956), Vol. 4, pp. 1–51.

[2] Schlichting, H., *Boundary Layer Theory* (McGraw-Hill Book Co. Inc., New York, 1960), 4th ed., pp. 551–563.

[3] Tewfik, O. E., "Some characteristics of the turbulent boundary layer with air injection," AIAA J. **1**, 1306–1312 (1963).

[4] Klebanoff, P. S. and Diehl, Z. W., "Some features of artificially thickened fully developed turbulent boundary layers with zero pressure gradient," NACA TR 1110 (1952).

[5] Sparrow, E. M., Eckert, E. R. G., and Minkowycz, W. J., "Heat transfer and skin friction for turbulent boundary-layer flow longitudinal to a circular cylinder," J. Appl. Mech. **30**, 37–43 (1963).

Blowing Effects on Pressure Interaction Associated with Cones

N. A. Thyson* and E. E. H. Schurmann†
Avco Corporation, Wilmington, Mass.

THE injection of mass (blowing) into a boundary layer through means of ablation or forced injection can significantly alter the character of the boundary layer. The general effects are well known: alteration of boundary-layer profiles, increase in boundary-layer thickness, and reduction in skin friction and heat transfer. This analysis will be concerned with only one aspect of the blowing phenomena, namely, the pressure interaction on a cone possessing a boundary layer with ablation-type blowing. Presently, there are no closed-form analytical methods for predicting the pressure interaction with blowing similar to that given by Probstein[1] for the no-blowing case. An extension of the technique used by Probstein to define the pressure interaction with blowing satisfactorily in terms of an analogous interaction parameter seems unlikely. An available and rigorous approach is to solve the conventional boundary-layer equations and additional species equation, all equations being coupled through the thermodynamic and transport properties of the gaseous mixture.

Thus, an accurate description of the boundary layer is obtained, and, from this boundary-layer solution, the pressure interaction can then be calculated. This will be the general procedure to be followed in this analysis.

Figure 1 illustrates the flow-field model. Applying the continuity equation to the axisymmetric boundary layer gives

$$\frac{V_e}{U_e} = \frac{\rho_w V_w}{\rho_e U_e}\left(\frac{1}{1+(\delta/r)}\right) + \frac{d\delta}{dx}\left[1-\left(\frac{1}{1+(\delta/r)}\right)\right] + \frac{d\delta^*}{dx} - \frac{\delta-\delta^*}{\rho_e U_e r}\frac{d}{dx}(\rho_e U_e r)$$

Received July 9, 1963. This work was sponsored under U.S. Air Force Contract No. AF 04 (694)-264.

* Associate Scientist, Aerodynamics Section, Research and Advanced Development Division.

† Assistant Section Chief, Aerodynamics Section, Research and Advanced Development Division. Member AIAA.

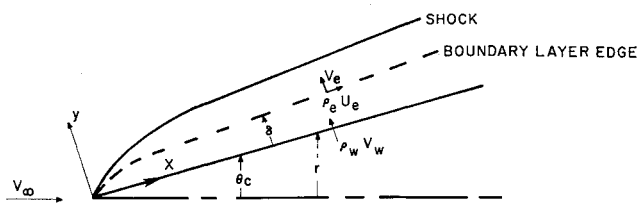

Fig. 1 Flow field about a cone.

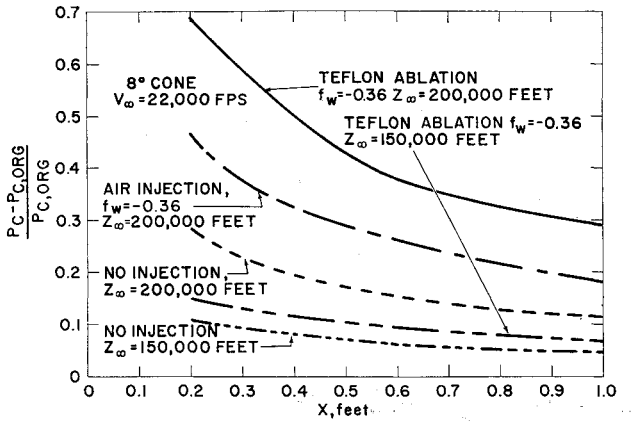

Fig. 2 Induced cone pressure.

where

$$\delta^* = \int_0^\infty \left(1 - \frac{\rho u}{\rho_e U_e}\right) dy$$

The foregoing expression for V_e/U_e may be simplified by employing the following assumptions. 1) $\delta \approx \delta^*$; and 2) $r \gg \delta$ (neglecting transverse curvature). Then

$$V_e/U_e = (\rho_w V_w/\rho_e U_e) + (d\delta^*/dx)$$

Mann[2] has derived the analogous expression for two-dimensional flow. The effective body shape or local cone angle then becomes

$$\theta_{\text{eff}} = \theta_{c,\text{org}} + (\rho_w V_w/\rho_e U_e) + (d\delta^*/dx)$$

The quantities $\rho_w V_w/\rho_e U_e$ and $d\delta^*/dx$ are obtained from the solution of the similar boundary-layer equations[3] wherein the gaseous composition of the boundary layer is assumed to be a binary mixture of equilibrium air and injected gas.

By using the noninteracting or original conical flow, the effective body shape may then be rewritten in terms of the similarity variables as

$$\theta_{\text{eff}} = \theta_{c,\text{org}} + \left(\frac{\rho_w}{\rho_e}\right)^{1/2}\left(\frac{\mu_w}{\rho_e U_e x}\right)^{1/2} \times \left[-\left(\frac{3}{2}\right)^{1/2} f_w + (6)^{-1/2}\int_0^\infty \left(\frac{\rho_e}{\rho} - \frac{u}{U_e}\right) d\eta\right]$$

where

$$f_w = -\rho_w V_w \left(\frac{2x}{3\rho_w \mu_w U_e}\right)^{1/2} \qquad \eta = \left(\frac{3U_e}{2\rho_w \mu_w x}\right)^{1/2} \int_0 \rho dy$$

and the resulting local pressure may then be obtained by employing the tangent-cone method. Of course, the rigorous procedure involves iterating to a final pressure distribution. However, for the cases analyzed in this analysis, the use of the original conical flow to compute the pressure interaction was sufficient. The induced pressure and pressure gradient had an insignificant effect on the slope, $d\delta^*/dx$, and on $\rho_w V_w/\rho_e U_e$.

Figure 2 illustrates induced pressure distributions on an 8° cone. Also of interest are the boundary-layer thickness and boundary-layer displacement thickness. Resulting values of these parameters are given in Table 1 and apply to the 1-ft cone station.

Table 1 Boundary-layer thickness and displacement thickness

Freestream conditions V_∞, fps	Z_∞, ft	Injected conditions	δ, ft	δ^*, ft
22,000	200,000	Teflon ablation	4.52×10^{-2}	3.45×10^{-2}
22,000	200,000	Forced air injection	3.81×10^{-2}	2.55×10^{-2}
22,000	200,000	Clean air, no injection	2.92×10^{-2}	1.8×10^{-2}
22,000	150,000	Teflon ablation	1.36×10^{-2}	1.06×10^{-2}
22,000	150,000	Clean air, no injection	1.05×10^{-2}	7.6×10^{-3}

Conclusions

1) There is a significant increase in the pressure with blowing as compared to the pressure interaction without blowing.

2) In general, for the case of blowing, the pressure interaction will be a function of the gas injection rate and a function of the injected gas itself.

References

[1] Probstein, R. F., "Interacting hypersonic laminar boundary layer flow over a cone," TR AF 2798/1, Div. Eng., Brown Univ., Providence, R. I. (March 1955).

[2] Mann, W. M., Jr., "Effective displacement thickness for boundary layers with surface mass transfer," AIAA J. **1**, 1181–1182 (1963).

[3] Van Tassell, W. and Pallone, A., "Similar solutions of the compressible laminar boundary-layer equations for air in equilibrium dissociation and ionization with and without air injection in the stagnation region," Avco RAD-TM-61-22 (June 1961).

Effects of Orthotropicity Orientation on Supersonic Panel Flutter

JOHN M. CALLIGEROS* AND JOHN DUGUNDJI†
Massachusetts Institute of Technology, Cambridge, Mass.

AN important structural aspect of the panel flutter problem is the effect of orthotropicity. Although generally it is felt that aligning stiffeners parallel to the airflow would give the maximum increase in the flutter boundary, it might be possible that some other angular orientation of the stiffeners would give a greater increase. Accordingly, this problem has been investigated for flat, rectangular, simply supported panels in a supersonic flow. This note is based on work reported in greater detail in Ref. 1 and is an extension of the basic problem of Hedgepeth.[2]

Consider the panel of Fig. 1. Using small deflection thin plate theory, the total potential energy π is given by[3]

$$\pi = \frac{1}{2}\int_0^a \int_0^b \left[D_{11}\left(\frac{\partial^2 w}{\partial x^2}\right)^2 + 2D_{12}\frac{\partial^2 w}{\partial x^2}\frac{\partial^2 w}{\partial y^2} + D_{22}\left(\frac{\partial^2 w}{\partial y^2}\right)^2 + 4D_{33}\left(\frac{\partial^2 w}{\partial x \partial y}\right)^2 + 4\frac{\partial^2 w}{\partial x \partial y} \times \left(D_{13}\frac{\partial^2 w}{\partial x^2} + D_{23}\frac{\partial^2 w}{\partial y^2}\right) - 2pw\right] dxdy \quad (1)$$

Received July 8, 1963. This research was supported by the Air Force Office of Scientific Research under Contract AF 49(638)-219.

* Senior Research Engineer, Aeroelastic and Structures Research Laboratory, Department of Aeronautics and Astronautics. Member AIAA.

† Associate Professor of Aeronautics and Astronautics. Member AIAA.